

Journal of Materials Chemistry A

Accepted Manuscript



This is an *Accepted Manuscript*, which has been through the Royal Society of Chemistry peer review process and has been accepted for publication.

Accepted Manuscripts are published online shortly after acceptance, before technical editing, formatting and proof reading. Using this free service, authors can make their results available to the community, in citable form, before we publish the edited article. We will replace this *Accepted Manuscript* with the edited and formatted *Advance Article* as soon as it is available.

You can find more information about *Accepted Manuscripts* in the [Information for Authors](#).

Please note that technical editing may introduce minor changes to the text and/or graphics, which may alter content. The journal's standard [Terms & Conditions](#) and the [Ethical guidelines](#) still apply. In no event shall the Royal Society of Chemistry be held responsible for any errors or omissions in this *Accepted Manuscript* or any consequences arising from the use of any information it contains.

Facile Synthesis of Highly Graphitized Porous Carbon Monolith with a Balance on Crystallization and Pore-Structure

Cite this: DOI: 10.1039/x0xx00000x

Received 00th January 2012,
Accepted 00th January 2012

DOI: 10.1039/x0xx00000x

www.rsc.org/

Shengyang Tao*^a, Yuchao Wang,^a Da Shi,^a Yonglin An,^a Jieshan Qiu,^b Yishan Zhao,^a Yan Cao ^a and Xuefang Zhang ^a

An efficient strategy is developed for producing hierarchically porous graphite (HPG) monolith with bimodal pore structure through confined graphitizing process with FeCl₃ as the catalyst. The micro space in silica microreactor is used for molding and protecting the carbon structure without collapse during crystallization. Especially, the confined graphitization approach is favorable for forming highly crystallized graphite materials with large specific surface at low preparation temperature. It balances the benefits of porous structure and degree of crystallization. Due to the outstanding physical and chemical properties, the graphitized porous carbon exhibits excellent electrochemical performances. HPG shows high sensitivity for use as sensing electrodes. Additionally, HPG also exhibits remarkable stabilization on capacitance at large current densities as a supercapacitor. There is hardly any loss in specific capacitance even with a charge current of 30 to 50 A g⁻¹.

Introduction

Unlike amorphous materials, crystals have precise periodicities over long-distance spaces formed by the regular arrangement of their atoms. Due to this highly ordered structure, crystal materials possess special physicochemical properties in terms of conductivity, magnetism and optical properties and are of tremendous value in various chemical processes such as sensors and catalysis.¹⁻³ With increasing application requirements as the driving force, chemists are focusing more attention on the fabrication of porous crystal inorganic materials with large specific surface areas. The ideal porous structure promotes diffusion and provides more reactive sites. However, it should be noted that large numbers of atoms will be rearranged during the crystallization process; as such, it remains a great challenge to avoid the collapse of the porous structure as the crystallinity increases and to balance the porous structure and degree of crystallization.^{4,5} Recently, Li et al. made use of mesopores as confined spaces to produce graphene on a large scale, and Yin et al. adopted silica spheres as templates to prepare porous anatase with a high surface area. These limited successes have demonstrated that the template method is an efficient way to obtain high-performance porous crystal materials, in which the template functions as a confined space and helps to protect the porous skeleton and control the crystallization.^{6,7}

Graphite consists of π - π parallel stacking of two-dimensional (2D) atomic crystals.⁸ It can be produced from various sources by chemical vapor deposition (CVD), high-temperature and/or high-pressure treatment, and catalytic graphitization.^{1, 9, 10} Of these methods, the catalytic approach can be carried out at lower temperatures, which helps to reduce cost. Some porous carbons with large specific surface areas have been prepared by catalytic graphitization with transition metals as the catalysts. However, most of the porous carbons are powders or particles, which require further processing before use.^{11, 12} Monolithic carbon, by contrast, is more suitable in applications- and has attracted much attention worldwide.¹³ There are a few reports on the preparation of the amorphous carbon monolith with hierarchical pore (HPC). But the fabrication of the monolith with both high crystallinity and well-defined porous structure is still a challenge.^{13, 14}

In this study, a facile method to fabricate hierarchically porous graphite (HPG) monolith by porous template and sol-gel methods with FeCl₃ as the catalyst. The macroporous skeleton and well-defined mesopores in HPG are formed via the complete reproduction of silica template (ST). The nanostructure and degree of graphitization can be tuned to some extent by varying the FeCl₃ content and heat-treatment temperature. In addition, the confined spaces configured by the ST are beneficial for the formation of the graphitized framework. It is an effective approach to balance the

crystallisation degree and porous framework by nanocasting in a suitable confined space. The as-made HPG monoliths show outstanding electrochemical performance.

Experimental details

Materials

Tetramethoxysilane (TMOS) was bought from the Chemical Factory of Wuhan University (Wuhan, China). Phenol (AR), formaldehyde solution (Formalin 37 wt %) and commercial graphite were bought from Aladdin Chemical Co., Ltd. (Beijing, China). The structure-directing agent, including P123 with an average molecular mass of 5800, F127 (Mw =12 600) and polyethylene glycol (PEG, Mw =10 000) were obtained from Aldrich Chemical Co. Inc. Nitric acid (AR) was purchased from Beijing Chemical Reagents Factory (Beijing, China). 25 wt % ammonia (AR), sodium hydroxide (AR), KCl (AR), $\text{FeCl}_3 \cdot 6\text{H}_2\text{O}$ (AR), potassium ferricyanide (AR), hydrochloric acid (AR), ethyl acetate and absolute alcohol were purchased from Fuyu Fine Chemical of Tianjin Co., Ltd. (Tianjin, China). HOPG (Highly Oriented Pyrolytic Graphite) was bought for Structure Probe, Inc. (USA). All the reagents mentioned above were used without further purification.

Synthesis of Resol Precursor

Phenol (1.22 g, 13 mmol) was melted at 40 °C and NaOH aqueous solution (0.26 g) was added dropwise with stirring. About 10 min later, Formalin (1.05 g, 37 wt %) containing formaldehyde (13.0 mmol) was added slowly at 75 °C, and keeping on stirring for 1 h. Cooled down to room temperature, the product was mixed with HCl solution in order to adjust the pH to neutral (about 7.0). The resultant resol was redissolved in ethanol for reserve, after removing the water via rotary evaporation below 50 °C.

Synthesis of Silica Template (ST)

The hierarchically porous silica monolith was prepared and modified by a sol-gel transition and the reaction with silylation reagent reported before.^{15, 16} The experimental details are shown in Supporting Information.

Fabrication of Monolithic Hierarchically Porous Graphite (HPG) and Monolithic Graphite (MG)

In a typical synthesis, tri-block copolymer F127 (1.0 g) was dissolved in ethanol (5 g). A certain amount of $\text{FeCl}_3 \cdot 6\text{H}_2\text{O}$ and resol (2.0 g) were in turn added with stirring at room temperature (RT) for 30 min. Then ST (1.2 g) was immersed in the homogeneous solution under static conditions at 25 °C for 24 h, and another 24 h was taken to evaporate ethanol at 25 °C. An initial thermal-treatment was carry out by heating the dry materials at 100 °C to lead further polymerization of phenolic resols. In the process of pyrolysis, the resulting composite monoliths were calcined at different temperature (900 °C /1000 °C /1100 °C /1200 °C) for 6 h under nitrogen at a heating rate of 1 °C min⁻¹ below 450 °C and 5 °C min⁻¹ above 600 °C.

Subsequently, the materials were treated with NaOH (2 M) solution to etch the silica and immersed in HCl (1.0 M) solution to remove iron element. Immediately, the samples were washed with deionized water several times to remove the residuals. Finally, the products labeled as HPG were obtained after drying in an oven at 100 °C over the night. The samples were signed as HPG-x-y, where x and y were assigned as the molar amount (mmol) of Fe in 1.0 g of resol, and the calcination temperature (100×y °C), respectively.

The monolithic graphite without ST (MG) was the sample obtained from the precursor solution without silica template. The resulted sol was poured into a polythene (PE) tubes. And the sample after calcinations was only washed with HCl in order to remove iron.

Characterization

The scanning electron microscopy (SEM) images were taken with a JEOL JSM-6700F field emission scanning electron microscope (20 kV). Transmission electron microscopy (TEM) and High-resolution TEM (HRTEM) analyses were carried out with Tecnai G220S-Twin equipment operating at 300 keV. X-Ray diffraction (XRD) patterns were obtained on a Rigaku D/MAX-2400 X-ray powder diffraction (Japan) using Cu K α radiation, operating at 40 kV and 10 mA. The size distribution of macropores was measured by a mercury porosimeter (PORESIZER-9320, Micromeritics Co., USA). The nitrogen adsorption and desorption isotherms were measured at 77 K using an ASAP 2010 analyzer (Micromeritics Co. Ltd.). Raman spectra were collected using a Nicolet Almega XR Raman system with 532 nm excitation laser from Thermo Fisher Scientific Inc. Thermal gravimetric analysis (TGA) was carried out using TA Q50 (TA Instruments, USA) from 25 to 850 °C at a heating rate of 5 °C min⁻¹ in air. The elements were analyzed by X-ray photoelectron spectroscopy (XPS, Shimadzu KROTAS AMICUS spectrometer).

Electrochemical measurement

The performance of the as-prepared materials worked as sensor was tested by the three-electrode system. The 0.1 M KCl aqueous solution used as the electrolyte. The reference electrode was saturated Ag/AgCl electrode in aqueous solution. The work electrode was a piece of HPG clamped by polished silver slice. A part of HPG (about 4 mm² in area and 0.9 mg) was come out from the silver. A polished glassy carbon (GC) electrode about 19.6 mm² (about 28.8 mg) was used as a comparison. The platinum sheet was employed as the counter electrode.

A standard three-electrode system was used to evaluate the electrochemical performance including cyclic voltammetry (CV), galvanostatic charge-discharge and electrochemical impedance spectroscopy (EIS) on a CHI model 660D electrochemical workstation (CH Instrument, Inc.) at RT. The working electrode was prepared by fixing a thin piece of as-prepared carbon samples on a platinum mesh. A platinum sheet and a saturated Ag/AgCl electrode were employed as the counter and the reference electrodes, respectively. A H₂SO₄

(2.0 M) aqueous solution was used as the electrolyte. The specific gravimetric capacitance (C in $F g^{-1}$) was calculated from the data of discharge process. EIS measurements were recorded with an alternating current (AC) amplitude of 10 mV in the frequency range of 10 mHz to 10 kHz. All the electrochemical test data were the averages of three times repeated to ensure the creditability of the results.

All the specific capacitances (C in $F g^{-1}$) were calculated according to the following equation.

$$C = \frac{It}{Vm} \quad (1)$$

where I is the discharge current (A), t is the discharge time (s), V is the potential change during discharge process, and m is the mass of active material in the work electrode (g).

$$E = \frac{1}{2} CV^2 \quad (2)$$

$$P = \frac{IV}{2m} \quad (3)$$

where C is the specific capacitance of the electrode material ($F g^{-1}$), I is the discharge current (A), V the potential change during discharge process (V), and m represents the mass of active materials (kg).

The assembly of simple capacitor device is described as below: Two piece of HPG-1.4-11 (about 36 mm^2) are used as the symmetric working electrodes with a separator (Celgard 2400) between them. The polished Pt sheets are applied as current collector. The above parts are sandwiched between the PE shells. The aqueous electrolyte, $2.0 \text{ mol L}^{-1} \text{ H}_2\text{SO}_4$ solution, is injected into the cell and sealed.

The prepared cells are connected in series with conductive alligator clips. After charging with the electrochemical workstation for several seconds (galvanostatic charge), the device can light the LED lamp.

Results and Discussion

The structural properties of HPG

For a typical run, a carbon source (phenolic resin), surfactant (F127), and catalyst (FeCl_3) are mixed and adsorbed in the ST. During and after the heat treatment, the resultant carbon monolith can maintain the regular shape of the ST without surface fissures or cracks (Fig. 1). The HPG also have some degree of mechanical strength and can be cut into small pieces easily. It is convenient to treat the carbon monolith into test samples for measurement without any additive and adhesive. The SEM examination reveals that all of the HPG monoliths exactly replicate the three-dimensional (3D) structure of the ST (Fig. 1b, and Fig. S1 in Supporting Information). The multi-macropore sizes are about 0.9 and $2.0 \mu\text{m}$ by mercury porosimeter, as Fig. S2 shown. In general, the carbon structure will suffer an obvious shrinkage of pore size during high-temperature carbonization. The collapse of framework may be unavoidable under the structure transformation from amorphous to graphitized without any support or protection. For the

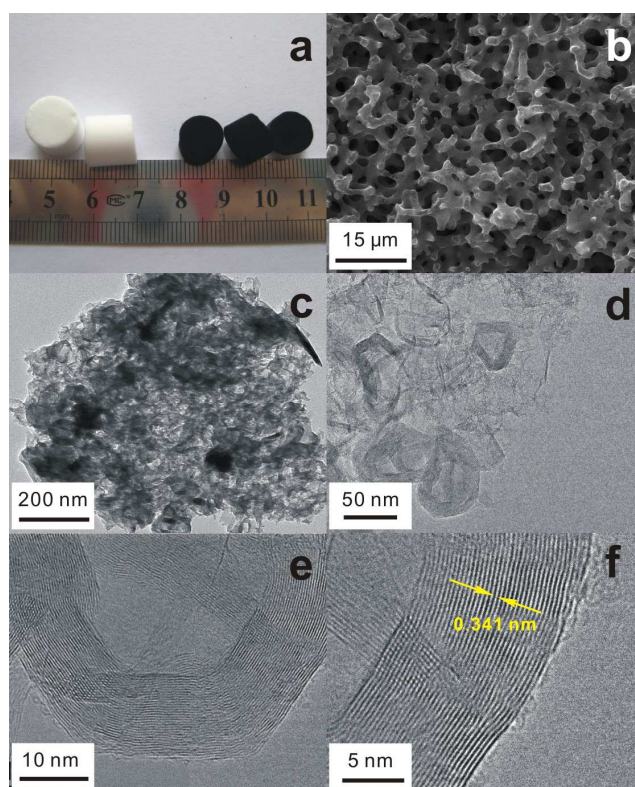


Fig. 1 Optical images of HPG-1.4-11 and ST (a), SEM (b), and HRTEM images (c-f) of HPG-1.4-11.

template effect of ST, the macroporous structure of the HPG to remain unchanged at different thermal-treatment temperatures and the catalyst contents.

The XRD and BET results show that the graphite degree and mesoporous structure of HPGs are sensitive to the temperature and catalyst. An HPG with an ideal crystalline mesoporous structure can be obtained using 1.4 mmol of catalyst and a calcination temperature of $1100 \text{ }^\circ\text{C}$. The wide-angle XRD examination reveals that the graphitization degree of the HPG increases with the calcination temperature at a catalyst amount of 1.4 mmol. As can be seen from Fig. 2a, the samples made at $1000 \text{ }^\circ\text{C}$ or higher show a sharp (002) peak, indicating the formation of graphitized structures. HPG-1.4-11 shows the characteristic peaks at ca. 26.4° , 42.6° , 44.5° , 54.6° , and 77.6° that correspond to the reflections of the graphitic planes (002), (100/101), (004), and (110), respectively.¹⁷ The high-intensity sharp (002) signal is generally regarded as the average stack height of the aromatic planes of carbon crystallite. The other observable bands including (100/110) and (004), can be attributed to the 2D and 3D graphitic structures.⁹ The Mering-Meire (g_p) index is used to quantitatively characterize the degree of similarity between a carbon material and a perfect single crystal of graphite:¹⁸

$$g_p = \frac{0.3440 \text{ (nm)} - d_{002}}{0.3440 \text{ (nm)} - 0.3354 \text{ (nm)}} \quad (4)$$

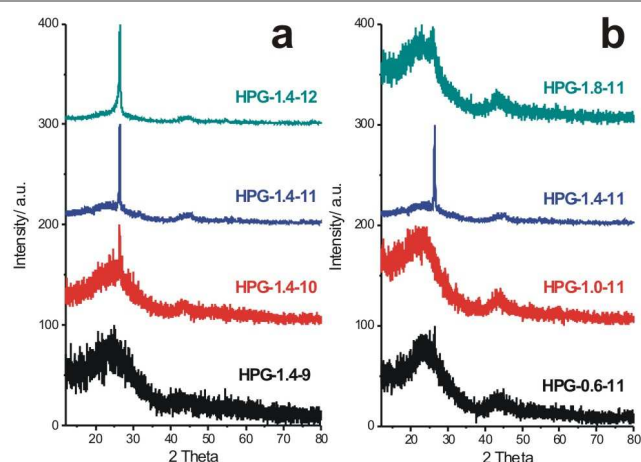


Fig. 2 Wide-angle XRD patterns for carbon samples at different calcination temperatures (a), and amounts of catalyst (b).

The interplanar spacing (d_{002}) can be obtained by $d_{002} = \lambda/2\sin\theta$. The index of HPG-1.4-11 is 0.67. A higher graphite index indicates a more ordered graphitic structure. At temperatures over 1100 °C, no obvious change in the degree of graphitization is observed (Fig. 2a). It should be noted that a temperature higher than 2000 °C is normally needed for the traditional methods of preparing graphitic materials.¹⁹⁻²¹ Obviously, a temperature of 1100 °C is much lower and easier to handle, which means that the approach adopted in our present work is mild and can save much energy.

The nitrogen sorption isotherms of the HPGs are shown in Fig. 3. The carbon material shows a broad H2-type hysteresis loop covering a p/p_0 range of 0.45-0.96 indicative of the existence of multi-size cylindrical mesopores, just as the pore size distribution in Fig. S3 in Supporting Information.²² Comparing with HPG, the sample (MG-11) synthesized without ST shows a similar shape of adsorption-desorption isotherm with a tinier hysteresis loop. Table 1 shows that the S_{BET} of the HPGs decreases from 886 to 312 $\text{m}^2 \text{g}^{-1}$ as the calcination temperature increases from 900 to 1200 °C. The degree of graphitization for HPG-1.4-11 and HPG-1.4-12 is similar, implying that 1100 °C is adequate for preparing HPG. For HPG-1.4-11, although the surface area drops slightly, but its

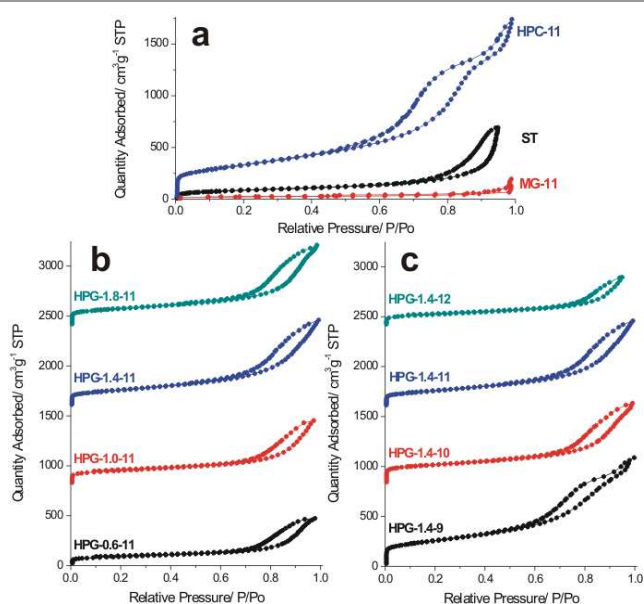


Fig. 3 N_2 adsorption-desorption isotherms of ST and carbon samples. The data are shifted by $800 \text{ cm}^3 \text{ g}^{-1} \text{ STP}$ relative to each other for clarity.

pore volume is superior to many graphitized monoliths reported in the literature.²³⁻²⁵ And the mean pore diameter is still large enough for substance transfer or diffusion inside. That is to say, ST plays a key role to sustain the carbon skeleton during the graphitization. The sample of HPG-0-11 without catalyst addition presents higher S_{BET} (about $1163 \text{ m}^2 \text{ g}^{-1}$) than HPG with FeCl_3 , because of the larger amount of mesopores. According to literatures,^{18, 25} the phenolic hydroxyl group can coordinate with Fe (III). The formation of the resin-Fe (III) complex changes the arrangement of resin chains, and causes an obvious decline of mesopore as the pore size distribution shown in Fig. S3. Less mesopores in HPG-x-11 leads to a smaller S_{BET} and pore volume finally.

As shown in Fig. 2b, the FeCl_3 catalyst has an obvious effect on the graphitization of HPG.²⁶ At lower loading amounts of FeCl_3 (0, 0.6, and 1.0 mmol), the characteristic peak at ca. 26.4° is broad and weak, meaning that no obvious crystalline structure is formed in the HPGs. This also implies that a small amount of catalyst cannot help to form an ideal graphitic

Table 1. Structural properties of the as-prepared materials

Sample	Template	FeCl_3 (mmol) ^a	Calcination temperature (°C)	S_{BET} ($\text{m}^2 \text{g}^{-1}$)	V_p ($\text{cm}^3 \text{g}^{-1}$)	D_p (nm)	FWHM (G-band) (cm^{-1})	I_D/I_G
ST				312	1.10	15.58		
MG-11	F127	1.4	1200	75	0.25	3.70	57	0.67
HPG-0-11	F127/ST	0	1100	1163	2.66	9.87		
HPG-0.6-11	F127/ST	0.6	1100	305	0.68	9.63		
HPG-1.0-11	F127/ST	1.0	1100	349	0.75	9.48		
HPG-1.4-11	F127/ST	1.4	1100	463	0.78	6.79	34	0.48
HPG-1.8-11	F127/ST	1.8	1100	585	1.15	8.61		
HPG-1.4-9	F127/ST	1.4	900	886	1.61	7.64	78	1.17
HPG-1.4-10	F127/ST	1.4	1000	704	1.28	8.15	68	1.03
HPG-1.4-12	F127/ST	1.4	1200	312	0.54	6.31	30	0.35

^a The amount of FeCl_3 corresponds to 1.0 g of phenolic resols.

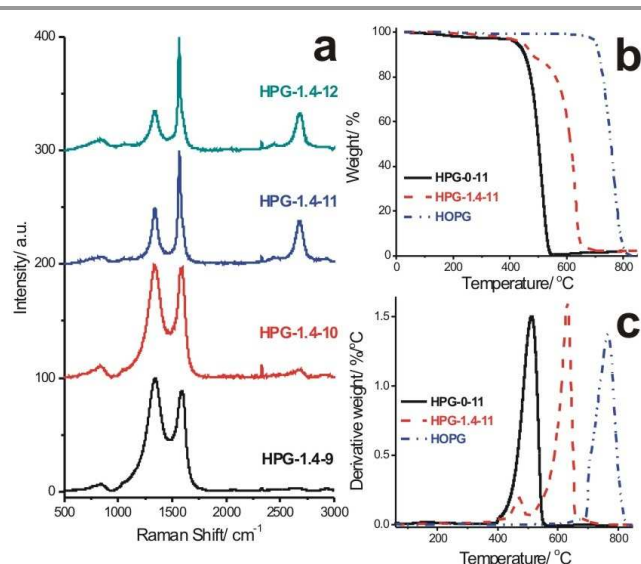


Fig. 4 Raman spectra (a), and TG (b) and DTG (c) profiles for carbon samples.

framework. When the FeCl_3 content further increases to 1.4 mmol, the peak at ca. 26.4° becomes strong and sharp, indicative of the formation of a fine graphitic structure. When more FeCl_3 is added (1.8 mmol), the peak becomes broad again, meaning a poor graphitization structure of the HPG. The variation in crystallization degree can be explained by the catalytic process. The formation of graphitic carbons with the assistance of transition metal particles usually takes place via a dissolution-precipitation mechanism.²⁷ It has been proven that Fe nanoparticles aggregate together easily and separate from the carbon matrix when excess catalysts are added.^{28, 29}

Other factors also affect the graphitization and structure of HPG. As shown in Fig. S4 in Supporting Information, the characteristic (002) peak gradually becomes stronger as the heat-treatment time increases. When the time exceeds 5 h, the peak signal-to-noise ratio is large in the XRD pattern. The (002) peak is strong and narrow, and few impurity peaks exist. When the phenolic resin (with F127 and FeCl_3) reacts in free space, not in the ST, the as-formed material (MG-11) has a considerable degree of graphitization. However, its surface area is only $75 \text{ m}^2 \text{ g}^{-1}$ with a pore volume of $0.25 \text{ cm}^3 \text{ g}^{-1}$, both of which are much smaller than those of HPGs prepared in the presence of STs. Obviously, the graphitized sample has less porosity with the absence of hard template, such as ST. The ST acts not only as a template to create some mesopores, but also as a barrier to prevent the collapse of mesoporous structure during the heat-treatment step. Just as the pore size distribution shown in Fig. S3, HPG-1.4-11 shows multi-size of mesopores in 3.7 nm and around 10 nm, respectively. While, the MG-11 only has the mesopores in 3.7 nm, which are created by F127. In HPG-1.4-11, the differential pore volume is about $0.15 \text{ cm}^3 \text{ g}^{-1} \text{ nm}^{-1}$ in 3.7 nm, but the MG-11's is only $0.09 \text{ cm}^3 \text{ g}^{-1} \text{ nm}^{-1}$. That is to say, without the protection of ST, the mesopores formed by F127 have been partly destroyed.

Consistent with the XRD result, the high graphitization structure is further confirmed by TEM (Fig. 1c-d) and HRTEM

imaging (Fig. 1e-f). Different from the amorphous carbon structure (Fig. S1i in Supporting Information), an aggregated nanocage structure can be observed from HPG with different curvatures and lengths, which means that the pore wall is formed by dense stacking of curved graphene layers. The regularly arranged graphene layers have a spacing of about 0.341 nm. This agrees with the formation of relatively large graphite crystallites in the carbonaceous pore walls.³⁰

Raman spectroscopy is a powerful analytical tool for quantifying the properties of carbon materials. Three major Raman signals can be identified, as shown in Fig. 4a. The peak at 1568 cm^{-1} , signed as the G-band, is associated with an E_{2g} mode of graphite, whereas the D-band at 1340 cm^{-1} corresponds to the breathing mode of κ -point phonons of A_{1g} symmetry for defected graphite.³¹ The degree of graphitization can be assessed by various criteria, including the FWHM (full width at half maximum) of the G-band and the D/G peak intensity ratio.^{32, 33} Among the samples, there are narrower G-band and lower I_D/I_G values with the increase in calcination temperature. High temperature is revealed to be a key factor in obtaining a high degree of graphitization with few defects in the carbon structure. The value of I_D/I_G is used to estimate the size of crystalline grains from the Tuinstra-Koenig equation:³⁴

$$\frac{I_D}{I_G} = \frac{C(\lambda)}{L_a} \quad (5)$$

where $C(\lambda) = (2.4 \times 10^{-10} \text{ nm}^{-3}) \times \lambda^4$. λ is the Raman excitation wavelength (532 nm in this work), and L_a is the coherence length representing the crystalline domain size. The L_a of HPG-1.4-11 is estimated to be at a quite high level of 39.2 nm. Compared with HPG-1.4-11, graphitization in MG-11 is relatively low, as indicated by a lower L_a of 28.6 nm (Table 1 and Fig. S5). Additionally, another peak signaled as the 2D band is detected at 2678 cm^{-1} . The shape of the HPG's 2D-band was assigned to a few layers of graphene,³⁵ i.e., the carbon wall is constituted by a few graphitic layers.

Graphite shows higher thermal stability than does amorphous carbon.³⁶ As Fig. 4b and c shown, there are two stages of weight loss at 400–500 °C and up to 500 °C in the TG curves, indicating the oxidation of amorphous and graphitic carbon, respectively.³⁷ The percentage of graphitic carbon can be estimated by the weight loss percentage above 500 °C. The data show that HPG-1.4-11 had a significantly high degree of graphitization of about 87%.

The electrochemistry properties of HPG

The graphitic HPG exhibits an outstanding sensing property as a porous electrode. Fig. 5a shows the CV curves of HPG-1.4-11 and a naked glassy carbon (GC) electrode in a 0.1 M KCl solution with 1.0 mM $\text{K}_3\text{Fe}(\text{CN})_6$. One pair of redox peaks of ferricyanide ions can be observed. Interestingly, the redox peaks of HPG-1.4-11 are much stronger and clearer than those of the GC, indicating that HPG-1.4-11 plays an important role in increasing the electroactive surface and providing the

conducting bridges for the electron transfer of $\text{Fe}(\text{CN})_6^{3-/4-}$. Due to its large specific surface area and low impedance, HPG-1.4-

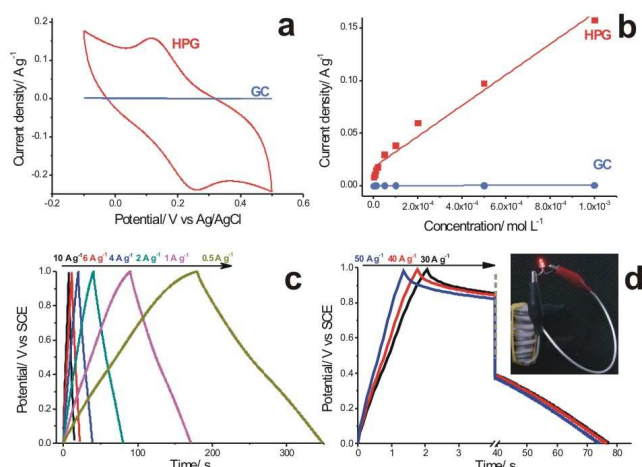


Fig. 5 Cyclic voltammograms of HPG-1.4-12 and bare glassy carbon (GC) electrode in a 1 mM $\text{K}_3\text{Fe}(\text{CN})_6$ aqueous solution with 0.1 M KCl at a scan rate of 50 mV s^{-1} (a), The peak current-concentration curves (b), Electrochemical performances of HPG-1.4-11 as the electrode material for a supercapacitor including galvanostatic charge-discharge curves (c), and The discharge curves at 1.0 A g^{-1} after charge processes in large current densities (d). The insert image is a simple capacitor device.

11 is beneficial for amplifying the electrochemical signal. This rise of redox peaks isn't caused by the presence of Fe impurities in HPG. The XPS result of HPG-1.4-11 reveals that the Fe, used for catalysis, has been removed completely in Fig. S6. As Fig. 5b shows, the peak-current values of HPG are considerably larger than the corresponding values of GC at different $\text{K}_3\text{Fe}(\text{CN})_6$ concentrations. The detection limit is as low as 0.18 μM .

Previous work¹³ confirmed that a hierarchically porous structure is beneficial for electrochemical supercapacitors. The crystalline carbon exhibits a high stability on the capacitance values under large current densities. The specific capacitance of HPG-1.4-11 is over 19 $\mu\text{F cm}^{-2}$, nearly the theoretical value of carbon materials (20 $\mu\text{F cm}^{-2}$).³⁸ Even when the current density increased as high as 20 A g^{-1} , the specific capacitance of HPG-1.4-11 still remained ca. 81.7 % to the value at 0.5 A g^{-1} . In Fig. 5c, the galvanostatic charge-discharge curves of the HPG-1.4-11 at different current densities are isosceles triangle shapes, suggesting ideal EDLC behavior.³⁹ As the current intensity increases, the shapes of the curves remain a triangle, indicating that the hierarchical structure can satisfy fast ion transfer/diffusion. The Nyquist plots in Fig. S7a show that the ESR of HPG-1.4-11 is much smaller than that of HPG-0-11. The lower resistance of the highly graphitized sample leads to better electrical conductivity.⁴⁰

Just as shown in Fig. 5d, HPG-1.4-11 shows hardly any loss in specific capacitance even with a charge current of 30 to 50 A g^{-1} (the discharge current density is 1.0 A g^{-1}). It means that the HPG can still remain the ideal capacitive performance after a quick charge process. Such evaluation criterion proves that the crystalline porous carbon has high practical application value for the stability of electrochemical performances. The Ragone

plots tested in two electrodes are shown in Fig. S7b. The HPG-1.4-11 has well energy densities with the increase in power densities. When the power density reaches 15000 W kg^{-1} , the energy density is still up to 21 Wh kg^{-1} . This is attributable to the high graphitization structure being beneficial to fast electron transfer, and because of this, the whole surface of the monolith can form an electric double layer in a short time at a large power density. Such performance is meaningful to practical applications. Using HPG-1.4-11 as electrodes, capacitors in series could light an LED lamp (operating voltage 3 V) after a 10-second charge at high current density (Fig. 5d insert).

Conclusions

In summary, we have developed an efficient strategy for producing an HPG monolith based on a confined graphitization approach. The crucial point in this strategy is the use of a porous silica microreactor for molding and protecting the structure during carbonization of phenolic resol with catalyst. Both the excellent porous and crystalline structure of HPG make it facile for use as a supercapacitor and sensing electrodes. The confined solid reaction approach used herein has several advantages: low preparation temperature, high crystallization, and a protected porous framework. Moreover, the procedure can be used to produce HPG materials on gram scale. We believe that our findings represent an important development in the preparation of high-quality graphitic materials on a large scale, which may significantly facilitate the use of graphite in a wide range of applications.

Acknowledgements

We are genuinely grateful to the National Natural Science Foundation of China (51273030) and the Fundamental Research Funds for the Central Universities (DUT14ZD217).

Notes and references

^a Department of Chemistry, Dalian University of Technology, Dalian, Liaoning, P. R. China. Fax: +86-411-84986035; Tel: +86-411-84986035; E-mail: taosy@dlut.edu.cn

^b Carbon Research Laboratory, Liaoning Key Lab for Energy Materials and Chemical Engineering, State Key Lab of Fine Chemicals, School of Chemical Engineering, Dalian University of Technology, Dalian, Liaoning, P. R. China.

Electronic Supplementary Information (ESI) available: The experimental details of silica template, SEM and TEM images of as-prepared samples, Raman spectrum of MG-11, electrochemical data of carbon samples. See DOI: 10.1039/b000000x/

- Z. Wu, W. Li, Y. Xia, P. Webley and D. Zhao, *Journal of Materials Chemistry*, 2012, **22**, 8835-8845.
- D.-W. Wang, F. Li, M. Liu, G. Q. Lu and H.-M. Cheng, *Angewandte Chemie-International Edition*, 2008, **47**, 373-376.
- F. B. Su, X. S. Zhao, Y. Wang, J. H. Zeng, Z. C. Zhou and J. Y. Lee, *Journal of Physical Chemistry B*, 2005, **109**, 20200-20206.
- B. Y. Xia, J. N. Wang, X. X. Wang, J. J. Niu, Z. M. Sheng, M. R. Hu and Q. C. Yu, *Advanced Functional Materials*, 2008, **18**, 1790-1798.

5. T. W. Kim, I. S. Park and R. Ryoo, *Angewandte Chemie-International Edition*, 2003, **42**, 4375-4379.
6. W. X. Zhang, J. C. Cui, C. A. Tao, Y. G. Wu, Z. P. Li, L. Ma, Y. Q. Wen and G. T. Li, *Angewandte Chemie-International Edition*, 2009, **48**, 5864-5868.
7. J. B. Joo, Q. Zhang, I. Lee, M. Dahl, F. Zaera and Y. D. Yin, *Advanced Functional Materials*, 2012, **22**, 166-174.
8. T. Hayashi, S. Hirono, M. Tomita and S. Umemura, *Nature*, 1996, **381**, 772-774.
9. S. B. Yoon, G. S. Chai, S. K. Kang, J. S. Yu, K. P. Gierszal and M. Jaroniec, *Journal of the American Chemical Society*, 2005, **127**, 4188-4189.
10. P. Su, L. Jiang, J. Zhao, J. Yan, C. Li and Q. Yang, *Chemical Communications*, 2012, **48**, 8769-8771.
11. A. H. Lu, W. C. Li, E. L. Salabas, B. Spliethoff and F. Schuth, *Chemistry of Materials*, 2006, **18**, 2086-2094.
12. H. Jiang, J. Ma and C. Z. Li, *Advanced Materials*, 2012, **24**, 4197-4202.
13. Y. C. Wang, S. Y. Tao and Y. L. An, *Microporous and Mesoporous Materials*, 2012, **163**, 249-258.
14. Y. C. Wang, S. Y. Tao, Y. L. An, S. Wu and C. G. Meng, *Journal of Materials Chemistry A*, 2013, **1**, 8876-8887.
15. Y. Wang, S. Tao and Y. An, *Journal of Materials Chemistry A*, 2013, **1**, 1701-1708.
16. T. Amatani, K. Nakanishi, K. Hirao and T. Kodaira, *Chemistry of Materials*, 2005, **17**, 2114-2119.
17. J. J. Li, R. J. Lu, B. J. Dou, C. Y. Ma, Q. H. Hu, Y. Liang, F. Wu, S. Z. Qiao and Z. P. Hao, *Environmental Science & Technology*, 2012, **46**, 12648-12654.
18. C. D. Liang, S. Dai and G. Guiochon, *Analytical Chemistry*, 2003, **75**, 4904-4912.
19. N. P. Wickramaratne, V. S. Perera, B. W. Park, M. Gao, G. W. McGimpsey, S. P. D. Huang and M. Jaroniec, *Chemistry of Materials*, 2013, **25**, 2803-2811.
20. M. N. Patel, X. Wang, D. A. Slanac, D. A. Ferrer, S. Dai, K. P. Johnston and K. J. Stevenson, *Journal of Materials Chemistry*, 2012, **22**, 3160-3169.
21. M. Beatriz Vazquez-Santos, E. Geissler, K. Laszlo, J.-N. Rouzaud, A. Martinez-Alonso and J. M. D. Tascon, *Carbon*, 2012, **50**, 2929-2940.
22. Y. H. Deng, C. Liu, T. Yu, F. Liu, F. Q. Zhang, Y. Wan, L. J. Zhang, C. C. Wang, B. Tu, P. A. Webley, H. T. Wang and D. Y. Zhao, *Chemistry of Materials*, 2007, **19**, 3271-3277.
23. M. Sevilla and A. B. Fuertes, *Carbon*, 2013, **56**, 155-166.
24. G. H. Wang and W. C. Li, *New Carbon Materials*, 2012, **27**, 55-60.
25. X. Y. He, L. Zhou, E. P. Nesterenko, P. N. Nesterenko, B. Paull, J. O. Omamogho, J. D. Glennon and J. H. T. Luong, *Analytical Chemistry*, 2012, **84**, 2351-2357.
26. A. Oya and H. Marsh, *Journal of Materials Science*, 1982, **17**, 309-322.
27. F. J. Derbyshire, A. E. B. Presland and D. L. Trimm, *Carbon*, 1975, **13**, 111-113.
28. S. J. Han, Y. K. Yun, K. W. Park, Y. E. Sung and T. Hyeon, *Advanced Materials*, 2003, **15**, 1922-1923.
29. L. Wang, C. Tian, B. Wang, R. Wang, W. Zhou and H. Fu, *Chemical Communications*, 2008, 5411-5413.
30. Z. J. Wang, R. R. Jia, J. F. Zheng, J. G. Zhao, L. Li, J. L. Song and Z. P. Zhu, *Acs Nano*, 2011, **5**, 1677-1684.
31. G. X. Wang, J. Yang, J. Park, X. L. Gou, B. Wang, H. Liu and J. Yao, *Journal of Physical Chemistry C*, 2008, **112**, 8192-8195.
32. A. G. Sadekar, S. S. Mahadik, A. N. Bang, Z. J. Larimore, C. A. Wisner, M. F. Bertino, A. K. Kalkan, J. T. Mang, C. Sotiropoulos-Leventis and N. Leventis, *Chemistry of Materials*, 2012, **24**, 26-47.
33. F. C. Tai, C. Wei, S. H. Chang and W. S. Chen, *Journal of Raman Spectroscopy*, 2010, **41**, 933-937.
34. F. Tuinstra and J. L. Koenig, *Journal of Chemical Physics*, 1970, **53**, 1126-1127.
35. D. C. Wei, Y. Q. Liu, Y. Wang, H. L. Zhang, L. P. Huang and G. Yu, *Nano Letters*, 2009, **9**, 1752-1758.
36. J. W. Long, M. Laskoski, T. M. Keller, K. A. Pettigrew, T. r. N. Zimmerman, S. B. Qadri and G. W. Peterson, *Carbon*, 2010, **48**, 501-508.
37. W. Jiang, G. Nadeau, K. Zaghbi and K. Kinoshita, *Thermochimica Acta*, 2000, **351**, 85-93.
38. H. Ji, X. Zhao, Z. Qiao, J. Jung, Y. Zhu, Y. Lu, L. L. Zhang, A. H. MacDonald and R. S. Ruoff, *Nature Communications*, 2014, **5**, 3317.
39. L. Z. Fan, Y. S. Hu, J. Maier, P. Adelhelm, B. Smarsly and M. Antonietti, *Advanced Functional Materials*, 2007, **17**, 3083-3087.
40. K. H. An, W. S. Kim, Y. S. Park, J. M. Moon, D. J. Bae, S. C. Lim, Y. S. Lee and Y. H. Lee, *Advanced Functional Materials*, 2001, **11**, 387-392.